Microchimica Acta (2019) 186:606
https://doi.org/10.1007/s00604-019-3709-x

ORIGINAL PAPER

An electrochemiluminescence immunosensor for the N-terminal brain natriuretic peptide based on the high quenching ability of polydopamine

Yanhua Zhao[1] · Li Li[1] · Lulin Hu[1] · Yong Zhang[1] · Dan Wu[1] · Hongmin Ma[1] · Qin Wei[1]

Received: 5 April 2019 / Accepted: 21 July 2019

Abstract

A sandwich-type electrochemiluminescence (ECL) immunosensor for the N-terminal brain natriuretic peptide (NT-proBNP) is described. The assay is based on the quenching of the ECL of graphite-like carbon nitride (g-C_3N_4) by polydopamine (PDA). Two-dimensional g-C_3N_4 is grown in-situ on titanium dioxide nanoflowers (TiO_2 NFs). The macroporous structure of the NFs enhances the interfacial stability of g-C_3N_4, and also promotes the ECL reaction of g-C_3N_4 with the co-reactant. The introduction of gold nanoparticles into the matrix further enhances the ECL and facilitates the immobilization of capture antibodies. The nanoquencher used to label the secondary antibody is synthesized by catalytic polymerization of dopamine in the presence of bimetallic NiPd nanoparticles. The nanoquencher preserves the high reactivity of polydopamine and quenches the ECL of the g-C_3N_4/TiO_2 system. Compared to other methods, the detection limit for NT-proBNP is decreased to 50 fg·mL^{-1}.

Keywords Nickel-palladium nanoparticles · Biosensor · Titanium dioxide nanoflowers · Catalytic polymerization · Carbon nitride · Heart failure biomarker

Introduction

It has been reported that N-terminal brain natriuretic peptide (NT-proBNP) is released under stress load in the heart. Its concentration can be used to reflect the degree of myocardial damage. NT-proBNP has been proved to be a sensitive and specific biomarker of heart failure. Therefore, it is urgent to develop a new and sensitive immunoassay for rapid diagnosis of NT-proBNP. Many methods for quantitative detection of NT-proBNP have been constructed, including electrochemistry [1], photoelectrochemistry, surface plasmon resonance (SPR) immunoassay [2], Surface-enhanced Raman spectroscopy (SERS) technology [3], and enzyme-linked immunosorbent assay (ELISA) [4]. However, these tests are quite complex, require cumbersome and expensive equipment.

Electrochemiluminescence (ECL) is a chemiluminescence triggered by electrochemical processes. As a new analytical technique, ECL does not require an additional light source. Although conventional ECL materials such as ruthenium complex [5] and luminol [6] have high ECL emission, there are also some disadvantages. At the same time, quantum dots (QDs) also have good ECL emission, but the luminescence mechanism of QDs [7] is uncertain. The use of semiconductor nanomaterials as luminescent probes enables the development and improvement of various detection strategies and sensing properties [8].

Graphite-like carbon nitride (g-C_3N_4), as a new kind of polymer semiconductor, has been widely used in photoelectric conversion [9] and ECL emitter [10]. g-C_3N_4 possesses good biocompatibility [11, 12] and stable band gap emission. However, g-C_3N_4 not only lacks good interfacial stability, but also is difficult to combine with biometric elements. It is usually recognize with biomolecule through doping elements [13] or surface functionalization [14]. Previously, it has been found that incorporation of dumbbell-like polyaniline-gold

Electronic supplementary material The online version of this article (https://doi.org/10.1007/s00604-019-3709-x) contains supplementary material, which is available to authorized users.

✉ Hongmin Ma
mahongmin2002@126.com

[1] Key Laboratory of Interface Reaction & Sensing Analysis in Universities of Shandong, School of Chemistry and Chemical Engineering, University of Jinan, Jinan 250022, China

Published online: 05 August 2019

(PANI-Au) heterogeneous nanomaterials. It is not only increases the interfacial stability of g-C_3N_4 but also enhances the ECL efficiency [15]. Among the semiconductor nanomaterials, titanium dioxide (TiO_2) [16] has received extensive attention due to its excellent photocatalytic performance and high redox potential [17]. Lui et al. synthesizes graphene coated graded TiO_2 nanocomposites to enhance photocatalytic performance [18]. In particular, flower-like titanium dioxide (TiO_2 NFs) is a layered material with a large size and a relatively large surface area. The effective composite two-dimensional nanostructure of TiO_2 NFs can help improve charge transport.

Signal-on and signal-off are commonly used in immunoassay. Additionally, all kind of ECL quenching strategies have been put forward based on the signal-off detection mode to improve the detection sensitivity [19]. Polydopamine (PDA), known as a fluorescence quenching agent, has been proved to build sensing strategies [20]. However, the enhancement strategy on PDA-based ECL annihilation capacity is few reported [21]. PDA as a melanin-like biopolymer is formed by oxidative polymerization of dopamine (DA), which contains large amounts of hydroxyl and amino functional groups [22–24]. In alkaline environment, the self-polymerization of DA is close with the oxidation of catechol. But the rate of DA self-polymerization is slow and takes a long time. Additionally, Li et al. reported that the addition of horseradish peroxidase (HRP) can make DA ultra-fast polymerization deposition [25]. However, the preparation and activity of enzymes restrict the practical application of this method. Therefore, artificial mimetic enzymes with catalytic activity become good substitutes. Wang et al. find that nickel-palladium hollow nanoparticles (NiPd) synthesis using nickel nanospheres as a sacrificial template not only have triple enzyme mimicking activity, but also possess high stability and good repeatability [26].

In this study, a high-efficiency quenching ECL immunosensor for NT-proBNP detection is designed base on the application of rapid catalytic synthesis of PDA by mimic enzymes (Scheme 1). As a sensing platform, TiO_2 NFs@g-C_3N_4 (TiO_2 NFs@CN) is synthesis by high-temperature calcination. The two-dimensional g-C_3N_4 grows on the surface of TiO_2 NFs to enhance the interfacial stability of g-C_3N_4, thereby increasing the ECL strength of g-C_3N_4. The introduction of gold nanoparticles (Au NPs) not only enhances the conductivity of luminescent materials, but also enhances the ECL signal and facilitates the immobilization of biomolecules. Besides, NiPd with peroxidase activity can catalyze the polymerization of DA to form PDA, which greatly increases the polymerization rate. PDA shows a strong quenching ability for the ECL signal of g-C_3N_4, which can be combined with immunoassay to improve the detection sensitivity of ECL immunosensors.

Experimental section

Materials and reagents

Tetrabutyl titanate (TBOT) is purchased from Sinopharm Chemical Reagent Co., Ltd. (Shanghai, China, http://www.macklin.cn/). NT-proBNP (Ag) and anti-NT-proBNP (Ab_1 and Ab_2) are purchased from the Shanghai Linc-Bio Science Co. Ltd. (Shanghai, China, http://www.linc-bio.com/). The other details are displayed in electronic supporting material (ESM).

Apparatus

Transmission electron microscopy (TEM) images are measured from a JEOL-2100F TEM (Japan). X-ray power diffraction (XRD) is measured through D8 advance X-ray diffractometer (Bruker AXS, Germany). The other details are displayed in ESM.

Synthesis of TiO_2 nanoflowers (NFs)

The TiO_2 NFs were synthesis in the light of the previous reported method through simply modification [18]. The syntheses details are described in the ESM.

Synthesis of TiO_2 NFs@CN and TiO_2 NFs@CN-Au nanocomposites

The syntheses details are described in the ESM.

Synthesis of nickel-palladium nanoparticles (NiPd)

The NiPd were synthesis in terms of the previous reported literature through simply modification [26]. The describe syntheses detail in the ESM.

Measurement procedure

The immunosensors incubate with different concentrations of NT-proBNP is placed in an ECL detector cell containing 10 mL of pH 7.4 PBS (0.1 mol·L^{-1}) and 0.1 mol·L^{-1} $K_2S_2O_8$ (include 0.1 mol·L^{-1} KCl) by CV method. The ECL signal is recorded via the MPI-F flow-injection chemiluminescence detector, and the voltage of the photomultiplier tube (PMT) is set at 700 V. The ECL signal measured potential is set as −1.6 ~0 V, and the rate is 0.1 V·s^{-1}.

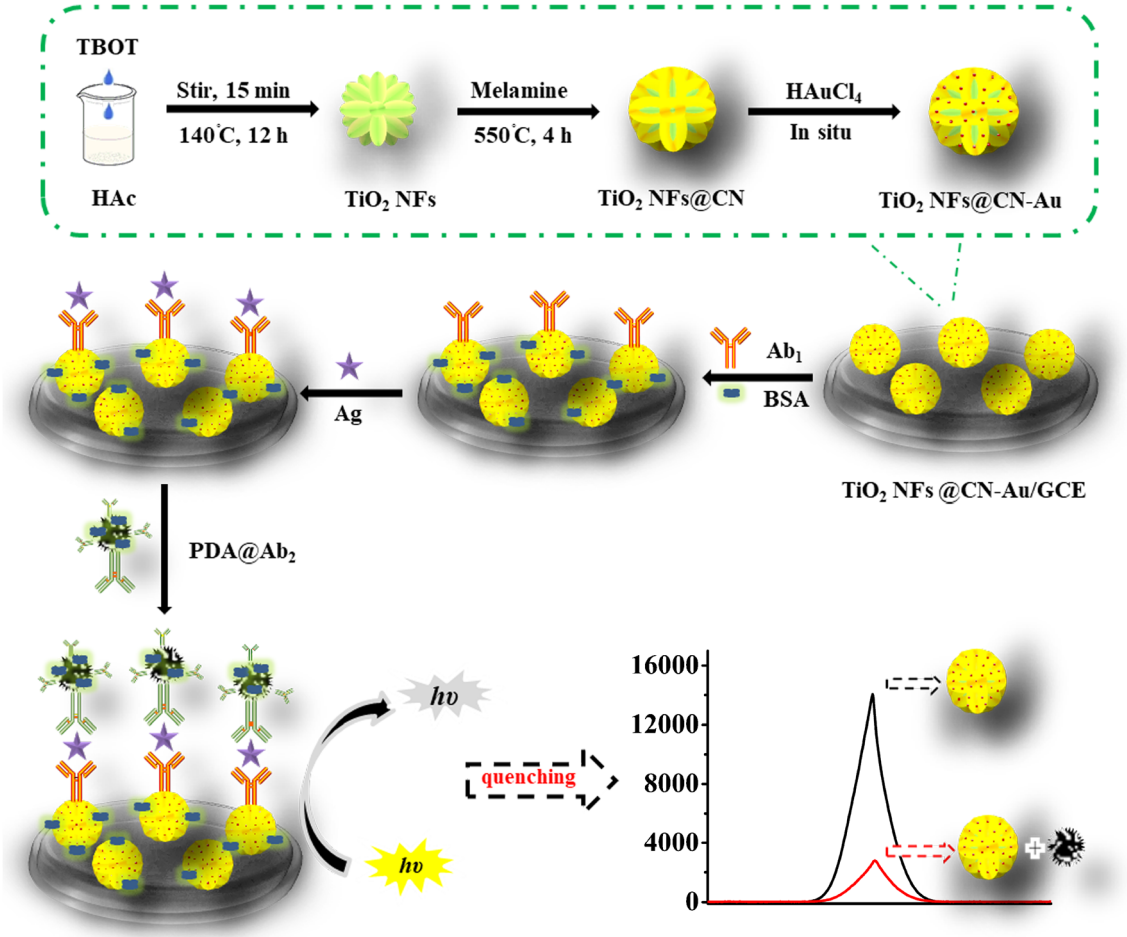

Scheme 1 The construction program of the ECL immunosensor

Results and discussion

Choice of materials

Compared with other carbon materials, g-C_3N_4 has been proved to be an ideal ECL emitter due to its highly adjustable electronic and optical properties. In this work, the flower-like structure of TiO_2 has a large specific surface area and porosity, which provides a larger binding site for material binding. In addition, it has good thermal stability and can withstand high temperature calcination. The space structure of g-C_3N_4 is increased by synthesizing on its surface. The contact area with the co-reaction reagent is promoted, and the signal intensity of g-C_3N_4 is enhanced. This provides a good basis for the construction of the sensor.

Characterization of TiO_2 NFs, TiO_2 NFs@CN and TiO_2 NFs@CN-Au

The morphological structures of materials are characterized using various means. It is apparent shown that the TiO_2 exhibits flower-like structure in Fig. 1a and Fig. S1. By calcining the mixture of TiO_2 NFs and dicyandiamide at high temperature, it can be clearly seen from Fig. 1b that a large amount of sheet-like substance is uniformly distributed on the surface of TiO_2 NFs. As shown in Fig. 1c, the surface of TiO_2 NFs@CN is loaded with abundant Au NPs. Besides, the crystal structure of the material is inferred by XRD (Fig. 1g). It can be seen that TiO_2 NFs (curve a) have an unknown crystal structure. While the annealed TiO_2 NFs form an obvious anatase phase (curve b) which consistent with previous literature [26]. The XRD peak at 27.6° (002) (curve c) is a characteristic peak of g-C_3N_4, and the peaks at 38.2° and 44.4° equivalent the 111 and 200 planes of Au. The composition of TiO_2 NFs@CN-Au is measured by XPS. It manifests that the composite contains Ti, O, C, N, and Au (Fig. S2). It can be seen from the BET diagram (Fig. 1h) that TiO_2 NFs (curve a) possesses porous structures and large specific surface area, which provides sufficient loading sites for two-dimensional carbon nitride. It can be also proved that the specific surface area of TiO_2@CN (curve c) is larger than g-C_3N_4 (curve d). As shown in Fig. 1d, it can be inferred that NiPd is a hollow structure. It can be inferred from

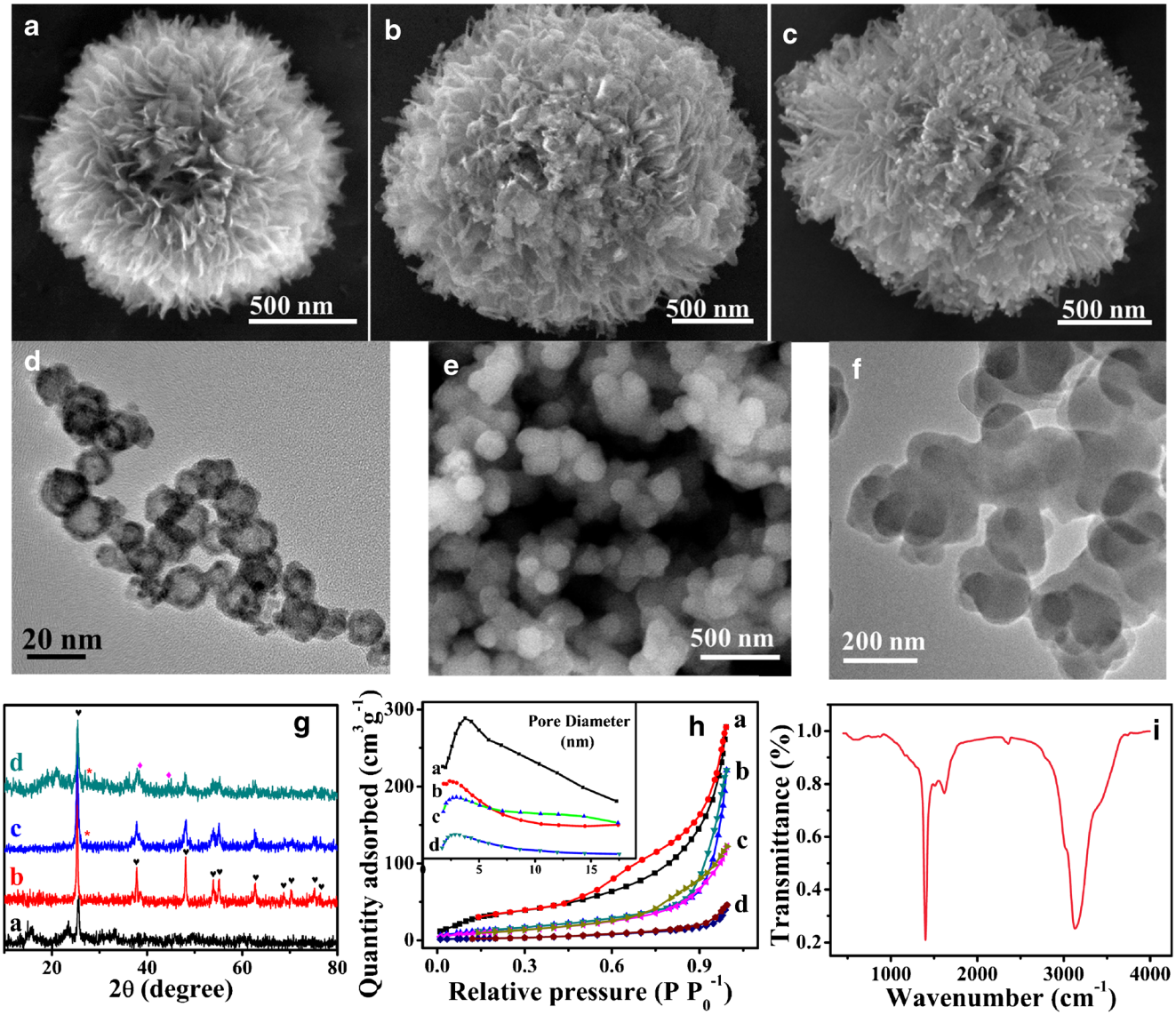

Fig. 1 **a-c** The magnified SEM image of TiO_2 NFs, TiO_2 NFs@CN and TiO_2 NFs@CN-Au; **d** TEM image of NiPd; **e-f** SEM and TEM image of PDA; **g** XRD spectra of (a) TiO_2 NFs, (b) annealed TiO_2 NFs, (c)TiO_2 NFs@CN, (d) TiO_2 NFs@CN-Au; (h) BET spectra of (a) TiO_2 NFs, (b) the annealed TiO_2 NFs, (c) TiO_2 NFs@CN, (d) g-C_3N_4; (i) The FT-IR spectra of PDA

the SEM (Fig. 1e) and TEM (Fig. 1f) that the product of NiPd catalyzes DA polymerization which exhibits a uniform spherical shape. Figure 1i shows the product possesses two remarkably characteristic absorption peaks at 1460 cm^{-1} and 3100 cm^{-1}, illustrating that PDA is synthesis successfully.

The verification of catalytic polymerization and ECL behaviors of TiO_2 NFs@CN-Au

To characterize the effect of NiPd on DA catalytic reactions a series of experimental studies are carried out. As shown in Fig. 2a, it is worth mentioning that compare with the self-polymerization reaction of DA, NiPd can rapidly catalyze DA polymerization in the presence of H_2O_2. This is attributed to the fact that NiPd can catalyze the rapid oxidation of some organic compounds in the presence of H_2O_2 [26]. In addition, the optimum pH of DA catalyzes by NiPd is selected (Fig. S7). The effect shows that the reaction is gradually raised with the increase of pH value, and the reaction doesn't change much when the pH reaches 9.0. And then pH 9.0 is selected as the optimum pH. Under optimal test conditions, it can be seen that the DA polymerization is completed after 60 min (Fig. 2b). Therefore, the best reaction time of 60 min is chosen in succeeding test.

For further verification the ECL performance of nanocomposites, the ECL response of different materials modified GCE under the same conditions are compared. As illustrates in Fig. 2c, the bare GCE has no significant ECL

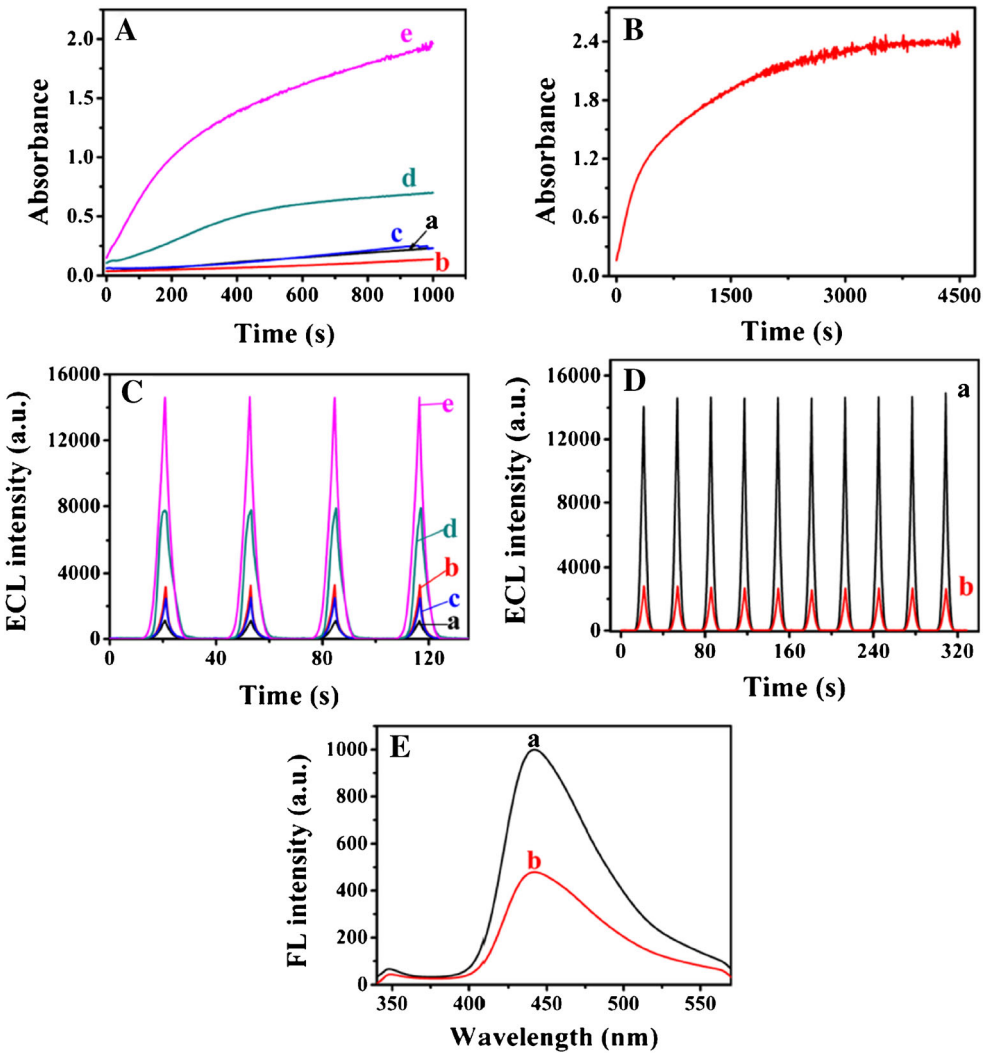

Fig. 2 **a** The absorbance-time spectra of the different reaction (a: DA, b: DA + H_2O_2, c: NiPd+ H_2O_2, d: NiPd+DA, e: NiPd+ DA + H_2O_2); **b** The catalytic polymerization of DA; **c** The ECL response of the GCE modified with different materials (a: GCE, b: TiO_2 NFs, c: the annealed TiO_2 NFs, d: TiO_2 NFs@CN, e:TiO_2 NFs@CN-Au); **d** ECL intensity of TiO_2 NFs@CN-Au (curve a) and TiO_2 NFs@CN-Au/PDA (curve b). (E) Fluorescence spectra of g-C_3N_4 (curve a) and the mixture solution of g-C_3N_4 and PDA (curve b) ($n = 5$)

emission. The ECL signal of TiO_2 NFs (curve b) and annealed TiO_2 NFs (curve c) are lower. When TiO_2 NFs@CN is dropped onto the electrode, there is a markedly enhanced ECL emission because g-C_3N_4 successfully grows on TiO_2 NF, forming a well-matched band structure that improves electron transfer (Fig. S6). Au NPs reduces the electron transfer barrier between TiO_2 NFs@CN and GCE, which accelerates the electron/hole injection rate, thereby increasing the ECL emission efficiency of TiO_2 NFs@CN.

Herein, TiO_2 NFs@CN luminophores are cathodic ECL with the presence of $K_2S_2O_8$ as co-reaction reagent. First, the energy of the electrons rises with the cathodic polarization of the potential, and then high-energy electrons are introduced into the conduction band (CB) of TiO_2 NFs@CN (Eq. 1)). At the same time, dissolves oxygen and $K_2S_2O_8$ get electrons to generate free radicals (Eq. 2 and Eq. 3). Next, the free radical interacts with TiO_2 NFs@CN to inject holes into the valence band (VB) of TiO_2 NFs@CN. Subsequently, the electrons inject in the CB and the holes in the VB are quenched to form TiO_2 NFs@CN* (Eq. 4 and Eq. 5). Finally, TiO_2 NFs@CN* returns to the TiO_2 NFs@CN and emits ECL (Eq. 6) [27].

$$TiO_2NFs@CN + e^- \rightarrow TiO_2NFs@CN^{\bullet -} \quad (1)$$

$$O_2 + H_2O + e^- \rightarrow OH^- + {}^{\bullet}OH \quad (2)$$

$$S_2O_8{}^{2-} - e^- \rightarrow SO_4{}^{\bullet -} + SO_4{}^{2-} \quad (3)$$

$$TiO_2NFs@CN^{\bullet -} + {}^{\bullet}OH \rightarrow TiO_2NFs@CN^* \quad (4)$$

$$TiO_2NFs@CN^{\bullet -} + SO_4{}^{\bullet -} \rightarrow TiO_2NFs@CN^* \quad (5)$$

$$TiO_2NFs@CN^* \rightarrow TiO_2NFs@CN + h\upsilon \quad (6)$$

The annihilation effect of PDA on ECL of TiO_2 NFs@CN-Au is confirmed in Fig. 2c. When PDA is modified on the TiO_2 NFs@CN-Au/GCE, the ECL signal is rapidly dropped. To verify this phenomenon, the fluorescence (FL) of g-C_3N_4 and PDA is tested. Available from Fig. 2e, the fluorescence intensity of mixture solution of g-C_3N_4 and PDA (curve b) is significantly lower than g-C_3N_4 (curve a). This proves that the

PDA has FL quenching ability for g-C_3N_4. Hence, the quinone units of PDA can quench the ECL signals of g-C_3N_4, resulting in a decrease in ECL signal.

Optimization of method

The following parameters were optimized: (a) sample pH value; (b) concentration of TiO_2; (e) concentration of $K_2S_2O_8$. Respective data and Figures are given in the Electronic Supporting Material. The following experimental conditions are found to give best results: (a) best sample pH value: 7.4; (b) optimal concentration of TiO_2: 1 mg·mL^{-1}; (c) optimal concentration of $K_2S_2O_8$: 100 mmol·L^{-1}.

Characterization of the designed immunosensors

Layer modification is an effective means to verify the successful construction of immunosensors. Observed from Fig. 3a, the bare GCE shows a tiny ECL intensity (curve a). Whlie the electrode is dropped by TiO_2 NFs@CN-Au, an excellent strong ECL signal is emerged (curve b). This result indicates that the substrate has a good ECL response. When Ab_1, BSA and NT-proBNP are immobilized on TiO_2 NFs@CN-Au/GCE, the ECL signal gradually decreases (curve c ~ e). Since the transmission of the interface electrons is hindered, the amount of diffusion of the co-reacting reagent to the electrode surface is greatly reduced. When PDA@Ab_2 is modified, the ECL signal (curve f) reduces greatly. It is mainly because the annihilation effect of the PDA greatly reduces the ECL intensity of the emitter. The above experimental results confirm that the construction of the immunosensor is successful.

The electrochemical impedances spectroscopy (EIS) is useful way to investigate whether the immunosensor is successfully constructed. It is performed through an electrochemical workstation (CHI 760E Chenhua Instrument Company, Shanghai, China) with a three-electrode system in 2.5 mmol·L^{-1} $[Fe(CN)_6]^{3-/4-}$ solution containing 0.1 mol·L^{-1} KCl. The frequency range is 0.1–10^5 Hz with amplitude of 5 mV. Figure 3b shows EIS map of the constructed sensor. The bare GCE has a small semicircular domain (curve a) because of the free electron transfer process. After TiO_2 NFs@CN-Au is modified to the electrode, there is a small impedance value (curve b) due to the properties of the semiconductor nanocomposites [28]. Subsequently, with the gradual modification of Ab_1, BSA,

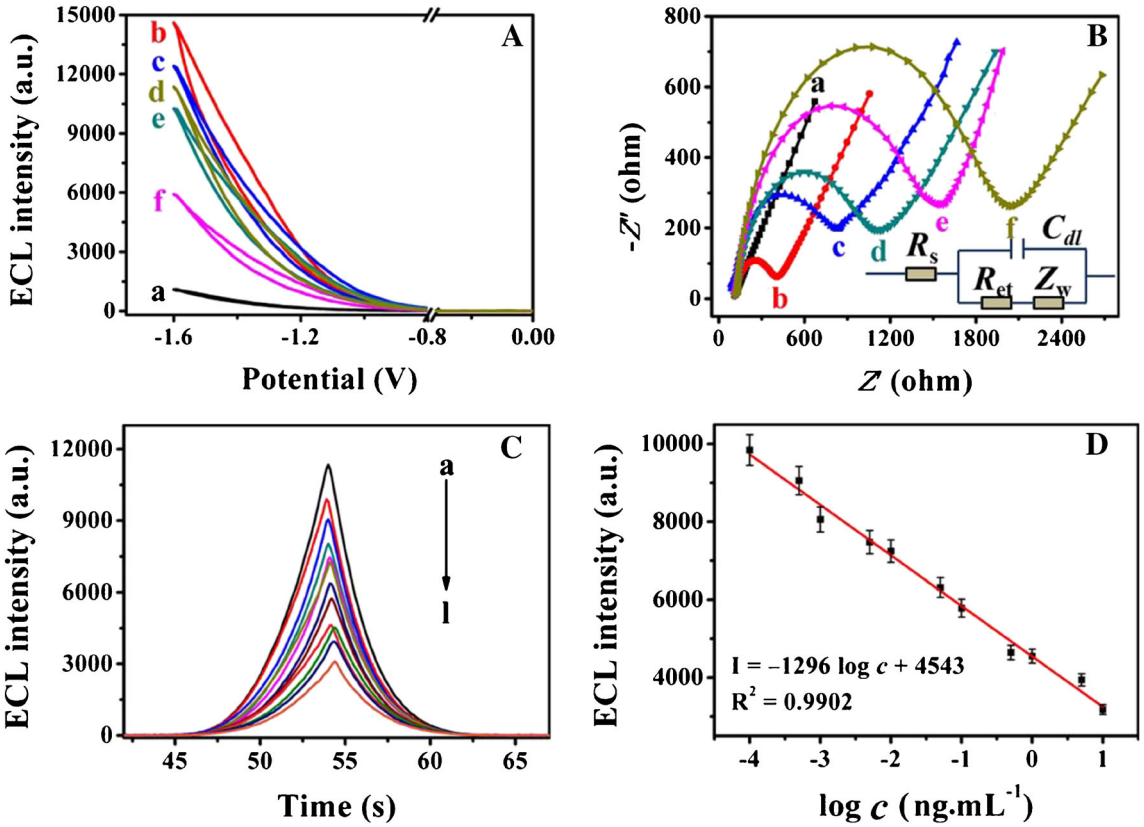

Fig. 3 **a** ECL responses and **b** EIS: GCE (curve a), TiO_2 NFs@CN-Au/GCE (curve b), Ab_1/TiO_2 NFs@CN-Au/GCE (curve c), BSA/Ab_1/TiO_2 NFs@CN-Au/GCE (curve d), NT-proBNP/BSA/Ab_1/TiO_2 NFs@CN-Au/GCE (curve e) and PDA-Ab_2/NT-proBNP/BSA/Ab_1/TiO_2 NFs@CN-Au/GCE (curve f) (NT-proBNP, 0.1 ng·mL^{-1}). **c** ECL signal of the different concentrations of NT-proBNP: (a) 0, (b) 0.0001, (c) 0.0005, (d) 0.001, (e) 0.005, (f) 0.01, (g) 0.05, (h) 0.1, (i) 0.5, and (j) 1.0, (k) 5.0 and (l) 10 ng·mL^{-1}. **d** Calibration plot for NT-proBNP determination

Table 1 Comparison of different methods for the detection of NT-proBNP

Method	Linear range	Detection Limit	Reference
Electrochemical	0.014 ~ 15 ng·mL^{-1}	4 pg·mL^{-1}	[29]
Microfluidic immunoassay	0.005 ~ 4 ng·mL^{-1}	3 pg·mL^{-1}	[1]
Surface-enhanced Raman spectroscopy	1 fg·mL^{-1} ~ 1 ng·mL^{-1}	0.75 fg·mL^{-1}	[3]
Photoelectrochemical	0.0008 ~ 45 ng·mL^{-1}	0.32 pg·mL^{-1}	[30]
Photoelectrochemical	0.01 ~ 50 ng·mL^{-1}	3.7 pg·mL^{-1}	[31]
ECL	0.01 ~ 100 pg·mL^{-1}	3.86 fg·mL^{-1}	[32]
ECL	0.0001 ~ 10 ng·mL^{-1}	0.05 pg·mL^{-1}	This work

NT-proBNP and PDA-Ab_2 (curve c ~ f), the impedance values increase to varying degrees. This is because every step contains protein molecules, which hinders electron transfer from the electrode surface. The result proves that the sensor is built successfully. The inset in Fig. 3b is an equivalent circuit. The values are measured using ZSimWin software and shows in Table S1.

Performance of the ECL assay

Under the best test conditions, the ECL response of different concentrations of NT-proBNP is recorded. As can be seen in Fig. 3c, as the concentration of the analyte increase (0 ~ 10 ng·mL^{-1}), the ECL intensity decrease significantly. The ECL intensity is linear with the logarithm of NT-proBNP concentration (Fig. 3d). The linear equation is $I = -1296 \log [c] + 4543$, with a correlation coefficient of 0.9902, and the detection limit is 0.05 pg·mL^{-1} (S/N = 3). The results reveal that the designed ECL immunosensor is excellently sensitive. As shown in Table 1, the designed ECL immunosensor has a relatively wide detection range and a lower detection limit compared with other methods of detecting NT-proBNP. This reflects the potential application value of this strategy.

Stability, selectivity and reproducibility

Stability, selectivity and reproducibility are the crucial indicators for measuring the practical performance of immunosensor. Figure 4a shows the ECL response of this sensing strategy in 9 cycles of continuous scanning. It can be noticed that the immunosensor has an extremely stable ECL signal. In addition, interference experiments of the constructed sensors are performed in this work, in which

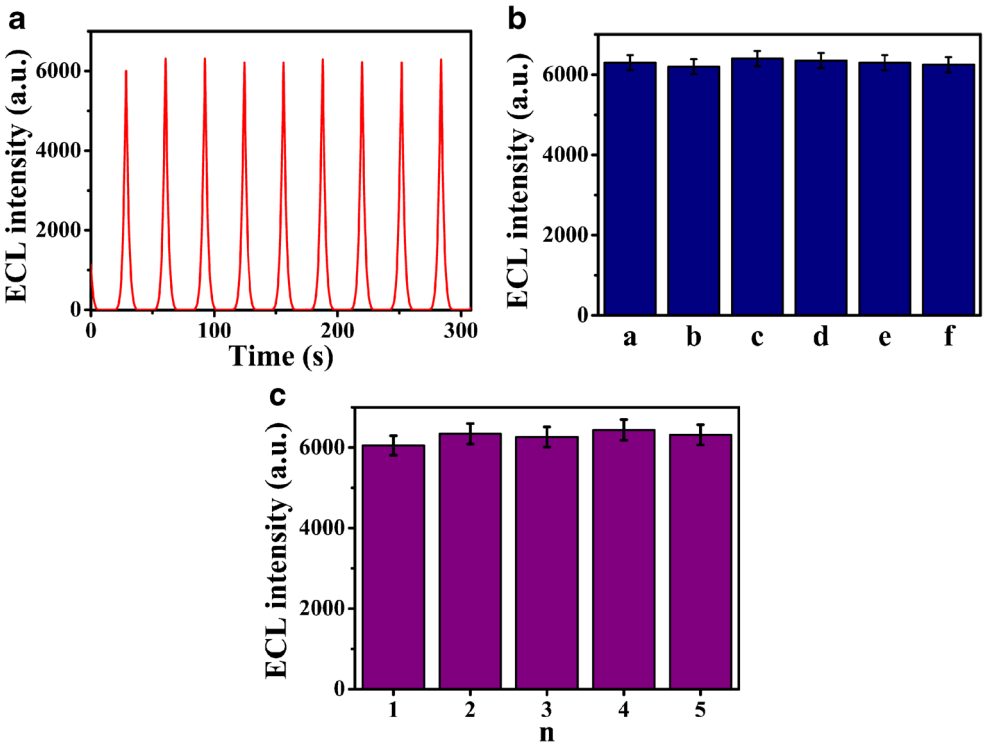

Fig. 4 **a** Stability of the ECL immunosensor; **b** Selectivity of the fabricated ECL immunosensor. (a) NT-proBNP; (b) NT-proBNP + CEA; (c) NT-proBNP + Human IgG; (d) NT-proBNP + SCCA; (e) NT-proBNP + BSA; (f) NT-proBNP + PSA; **c** Reproducibility of the ECL immunosensor. Error bar = SD (n = 5)

Table 2 The results of NT-proBNP determination in human serum

Content ($ng \cdot mL^{-1}$)	Added ($ng \cdot mL^{-1}$)	Mean ± SD ($n = 5$)($ng \cdot mL^{-1}$)	RSD (%)	Recovery (%)
0.62	0.1	0.718 ± 0.023	3.2	98.0
	1	1.618 ± 0.024	1.5	99.8
	5	5.634 ± 0.054	0.96	100.3

the NT-proBNP concentration is 0.1 $ng \cdot mL^{-1}$ and the interference concentration is 10 $ng \cdot mL^{-1}$. As shown in Fig. 4b, it can be observed that the constructed immunosensor shows a good selectivity for NT-proBNP (RSD = 2.9%, RSD < 5%). Furthermore, the reproducibility of the immunosensor is studied in Fig. 4c. Five electrodes of NT-proBNP (0.1 $ng \cdot mL^{-1}$) are tested in the same conditions, the relative standard deviation is 2.3% (RSD < 5%). The results reveal that the reproducibility of the designed immunosensor is within the acceptable range.

Application of the designed immunosensor

For further verify the feasibility of the designed immunosensor in practical applications, this task uses the standard recovery method to conduct a serum sample feasibility study on the designed immunosensor. At first, blood cells and other blood deposits in human blood (got from hospital) are removed by centrifugation. And then, the serum sample is diluted with PBS of pH 7.4. As shown in Table 2, standard NT-proBNP solutions at a concentration of 0.1 $ng \cdot mL^{-1}$, 1 $ng \cdot mL^{-1}$ and 5 $ng \cdot mL^{-1}$ are separately added to the serum samples, with an RSD range of 0.96 ~ 3.2% and recovery of 98 ~ 100.3%. The results show that the ECL immunosensor can be effectively applied to detect NT-proBNP in human serum samples.

Conclusions

A quenched-type ECL immunosensor is designed successfully based on TiO_2 NFs@CN-Au as solid light emitting platform and PDA as nanoquencher. The synergistic enhancement of TiO_2 NFs and Au NPs increased the ECL signal of g-C_3N_4 and promoted the immobilization of biomolecules. In addition, NiPd can rapidly catalyze the polymerization of DA into PDA, which greatly shortens the time-consuming reaction. What's more, PDA exhibits strong annihilation ability for the ECL signals of g-C_3N_4. The sensor possesses a good linear relationship in the NT-proBNP concentration range of 0.0001 ~ 10 $ng \cdot mL^{-1}$ with a lower detection limit. The ECL assay can sensitive and selective for the detection of NT-proBNP. In addition, we plan to design a ratiometric electrochemiluminescence assay based on the ratio of two signals.

Acknowledgments This work is supported by the National Natural Science Foundation of China (21675063, 21575050), the National Key Scientific Instrument and Equipment Development Project of China (No. 21627809), the Science and Technology Planning Project of Higher Education of Shandong Province (J16LC23), the Taishan Scholar Foundation of Shandong Province (Grant No. ts20130937).

Compliance with ethical standards The author(s) declare that they have no competing interests.

References

1. Liang W, Li Y, Zhang B, Zhang Z, Chen A, Qi D, Yi W, Hu C (2012) A novel microfluidic immunoassay system based on electrochemical immunosensors: an application for the detection of NT-proBNP in whole blood. Biosens Bioelectron 31(1):480–485
2. Teramura Y, Arima Y, Iwata H (2006) Surface plasmon resonance-based highly sensitive immunosensing for brain natriuretic peptide using nanobeads for signal amplification. Anal Biochem 357(2): 208–215
3. He Y, Wang Y, Yang X, Xie S, Yuan R, Chai Y (2016) Metal organic frameworks combining CoFe2O4 magnetic nanoparticles as highly efficient SERS sensing platform for ultrasensitive detection of N-terminal pro-brain natriuretic peptide. ACS Appl Mater Interfaces 8(12):7683–7690
4. Ding YD, Lei JY, Chen Y, Jin J (2010) A sandwich ELISA for assessment of pharmacokinetics of HSA-(BNP) fusion protein in mouse plasma. J Pharm Biomed Anal 51(3):658–663
5. Feng Y, Feng S, Wang N, Lei J, Ju H (2017) $Ru(bpy)_3^{2+}$ incorporated luminescent polymer dots: double-enhanced electrochemiluminescence for detection of single-nucleotide polymorphism. Anal Chem 89(14):7659–7666
6. Jiang X, Wang H, Wang H, Zhuo Y, Yuan R, Chai Y (2016) Self-enhanced N-(aminobutyl)-N-(ethylisoluminol) derivative-based electrochemiluminescence immunosensor for sensitive laminin detection using PdIr cubes as a mimic peroxidase. Nanoscale 8(15): 8017–8023
7. Yang X, Yu YQ, Peng LZ, Lei YM, Chai YQ, Yuan R, Zhuo Y (2018) Strong electrochemiluminescence from MOFs accelerator enriched quantum dots for enhancing sensing of trace cTnI. Analy Chem 90(6):3995–4002
8. Chen Y, Zhou S, Li L, Zhu JJ (2017) Nanomaterials-based sensitive electrochemiluminescence biosensing. Nano Today 12:98–115
9. Li X, Zhou Y, Xu Y, Xu H, Wang M, Yin H, Ai S (2016) A novel photoelectrochemical biosensor for protein kinase activity assay based on phosphorylated graphite-like carbon nitride. Anal Chim Acta 934:36–43
10. Chen W, Yao X, Zhou X, Zhao K, Deng A, Li J (2018) Electrochemiluminescence based competitive immunoassay for Sudan I by using gold-functionalized graphitic carbon nitride and Au/Cu alloy nanoflowers. Microchim Acta 185(5):275
11. Zhang X, Xie X, Wang H, Zhang J, Pan B, Xie Y (2012) Enhanced photoresponsive ultrathin graphitic-phase C_3N_4 nanosheets for bioimaging. J Am Chem Soc 135(1):18–21

12. Zhang XL, Zheng C, Guo SS, Li J, Yang HH, Chen G (2014) Turn-on fluorescence sensor for intracellular imaging of glutathione using g-C_3N_4 nanosheet–MnO_2 sandwich nanocomposite. Anal Chem 86(7):3426–3434
13. Chen L, Zeng X, Si P, Chen Y, Chi Y, Kim DH, Chen G (2014) Gold nanoparticle-graphite-like C_3N_4 nanosheet nanohybrids used for electrochemiluminescent immunosensor. Anal Chem 86(9): 4188–4195
14. Cao HX, Wang L, Pan CG, He YS, Liang GX (2018) Aptamer based electrochemiluminescent determination of bisphenol a by using carboxylated graphitic carbon nitride. Microchim Acta 185(10):463
15. Zhao Y, Liu Y, Li X, Wang H, Zhang Y, Ma H, Wei Q (2018) Label-free ECL immunosensor for the early diagnosis of rheumatoid arthritis based on asymmetric heterogeneous polyaniline-gold nanomaterial. Sensors Actuators B Chem 257:354–361
16. Su Y, Yang S, Liu W, Qiao L, Yan J, Liu Y, Zhang S, Fang Y Visible light photoelectrochemical sulfide sensor based the use of TiO_2 nanotube arrays loaded with Cu_2O. Microchim Acta 184(10): 4065–4072
17. Thamima M, Karuppuchamy S (2016) Synthesis, characterization and photocatalytic properties of rod-shaped titanium dioxide. J Mater Sci Mater Electron 27(1):458–465
18. Lui G, Liao JY, Duan A, Zhang Z, Fowler M, Yu A (2013) Graphene-wrapped hierarchical TiO_2 nanoflower composites with enhanced photocatalytic performance. J Mater Chem A 1(39): 12255–12262
19. Ma H, Zhao Y, Liu Y, Zhang Y, Wu D, Li H, Wei Q (2017) A compatible sensitivity enhancement strategy for electrochemiluminescence immunosensors based on the biomimetic melanin-like deposition. Anal Chem 89(24):13049–13053
20. Fan D, Zhu X, Zhai Q, Wang E, Dong S (2016) Polydopamine nanotubes as an effective fluorescent quencher for highly sensitive and selective detection of biomolecules assisted with exonuclease III amplification. Anal Chem 88(18):9158–9165
21. Xue H, Zhao J, Zhou Q, Pan D, Zhang Y, Zhang Y, Shen Y (2019) Boosting the sensitivity of a photoelectrochemical immunoassay by using SiO_2@polydopamine core-shell nanoparticles as a highly efficient quencher. ACS Appl Nano Mater 2:1579–1588
22. Liu Y, Zhao Y, Fan Q, Khan MS, Li X, Zhang Y, Ma H, Wei Q (2018) Aptamer based electrochemiluminescent thrombin assay using carbon dots anchored onto silver-decorated polydopamine nanospheres. Microchim Acta 185(2):85
23. Li H, Du W, Jiao L, Chen L, Ran B, Dong M, Qian Z (2017) Ultrasensitive simultaneous electrochemical immunoassay of acute myocardial infarction biomarkers using metal ion chelated polydopamine nanospheres. J Biomed Nanotechnol 13(10):1235–1242
24. Lai Y, Zhang C, Deng Y, Yang G, Li S, Tang C, He N (2019) A novel α-fetoprotein-MIP immunosensor based on AuNPs/PTh modified glass carbon electrode. Chin Chem Lett 30(1):160–162
25. Li J, Baird MA, Davis MA, Tai W, Zweifel LS, Waldorf KMA, Jr MG, Rajagopal L, Pierce RH, Gao X (2017) Dramatic enhancement of the detection limits of bioassays via ultrafast deposition of polydopamine. Nat Biomed Eng 1(6):0082
26. Wang Q, Zhang L, Shang C, Zhang Z, Dong S (2016) Triple-enzyme mimetic activity of nickel-palladium hollow nanoparticles and their application in colorimetric biosensing of glucose. Chem Commun 52(31):5410–5413
27. Cheng C, Huang Y, Tian X, Zheng B, Li Y, Yuan H, Xiao D, Xie S, Choi MMF, Chem A (2012) Electrogenerated chemiluminescence behavior of graphite-like carbon nitride and its application in selective sensing Cu^{2+}. Anal Chem 84(11):4754–4759
28. Zhai Q, Li J, Wang E (2017) Recent advances based on nanomaterials as electrochemiluminescence probes for the fabrication of sensors. Chemelectrochem 4(7):1639–1650
29. Serafín V, Torrenterodríguez RM, Gonzálezcortés A, García PDF, Sabaté M, Campuzano S, Yáñezsedeño P, Pingarrón JM (2018) An electrochemical immunosensor for brain natriuretic peptide prepared with screen-printed carbon electrodes nanostructured with gold nanoparticles grafted through aryl diazonium salt chemistry. Talanta 179:131–138
30. Feng J, Li F, Li X, Wang Y, Fan D, Du B, Li Y, Wei Q (2018) Label-free photoelectrochemical immunosensor for NT-proBNP detection based on La-CdS/3D $ZnIn_2S_4$/au@ZnO sensitization structure. Biosens Bioelectron 117:773–780
31. Fan D, Bao C, Liu X, Wu D, Zhang Y, Wang H, Du B, Wei Q (2018) A novel label-free photoelectrochemical immunosensor based on NCQDs and Bi_2S_3 co-sensitized hierarchical mesoporous SnO_2 microflowers for detection of NT-proBNP. J Mater Chem B 6(46):7634–7642
32. Zhang H, Han Z, Wang X, Li F, Cui H, Yang D, Bian Z (2015) Sensitive immunosensor for N-terminal pro-brain natriuretic peptide based on N-(aminobutyl)-N-(ethylisoluminol)-functionalized gold nanodots/multiwalled carbon nanotube electrochemiluminescence nanointerface. ACS Appl Mater Interfaces 7(14):7599–7604